Kovove Mater. 62 2024 275–283
DOI: 10.31577/km.2024.5.275

Fabrication of SiC and h-BN particle-reinforced Cu-Sn-Zn sliding alloy by powder metallurgy and characterization

Ahmet Oktay Devecili[1,2]*, Adem Bakkaloğlu[2], Yücel Gencer[3]

[1] *R&D Center, Hema Industry, Tekirdag, Turkey*
[2] *Metallurgical and Materials Engineering, Yildiz Technical University, Istanbul, Turkey*
[3] *Department of Materials Science and Engineering, Gebze Technical University, Kocaeli, Turkey*

Received 2 October 2023, received in revised form 16 October 2024, accepted 17 October 2024

Abstract

In this study, samples were produced by powder metallurgy, adding 0.25 wt.% h-BN and 0.25, 0.5, 1, 2, 4, and 5 wt.% SiC to Cu, Zn, and Sn metallic powder mixtures. The samples were mixed using high-energy mechanical alloying and compacted under a 400 N mm^{-2} pressure. Subsequently, they were sintered for 2 h at 820 °C in a controlled atmosphere furnace. Characterization processes included hardness measurement, XRD analysis, dimensional changes, and electron and optical microscopy. The results of the study revealed that the dimensional change after sintering increased initially with the addition of SiC and then decreased as the addition amount increased. XRD analysis identified characteristic peaks of the reinforcement materials and the metallic matrix. SEM analysis confirmed the distribution of h-BN and SiC within the metallic matrix. Wear resistance was significantly improved with increasing SiC addition in the 3 N load wear tests, remaining unchanged in the 1 N load wear tests. Furthermore, an increase in SiC content led to consistent friction coefficients at each stage of the wear test, while SiC-free samples exhibited load-dependent changes in friction coefficients.

K e y w o r d s: powder metallurgy, wear, mechanical alloying, SiC, h-BN

1. Introduction

This research on metal matrix composites, particularly in applications like sliding bearings, provides valuable insights into their low friction coefficient (COF), high wear resistance, and capacity to operate effectively at high temperatures. The most used metal matrix composites in sliding bearings have copper as their primary matrix material. Alloying elements such as Al, Pb, Si, Zn, and Sn are added to enhance their wear resistance and mechanical strength values. When alloyed with tin and zinc elements, copper-based metallic materials are preferred for sliding-bearing alloys primarily due to their low COFs, embeddability, and ease of manufacturing. However, their limited wear resistance can be a limiting factor in their usage. Furthermore, in high-temperature applications, ceramic reinforcement materials such as TiC, WC, Al_2O_3, BN_4, and SiC are employed alongside metallic alloying to enhance wear resistance, toughness, mechanical properties, and load-carrying capacities. However, it has been reported that the use of ceramic reinforcement materials can enhance wear resistance but may also increase COF. Solid lubricating additives are introduced alongside these materials to achieve low COF and ensure smooth operation in both lubricated and potentially dry conditions. The most commonly used solid lubricants include laminar structured materials like MoS_2, graphite, and h-BN derivatives. Due to their stability at high temperatures, graphite, h-BN, and MoS_2 are among the preferred solid lubricants. The very weak Van der Waals bonds between the layers in the structure of these solid lubricants can break under friction and wear, creating a sliding effect between two surfaces and contributing to a reduction in the COF. Some studies have also investigated the simultaneous addition of solid lubricating materials like graphite, MoS_2, and ceramic additives, which can contribute to wear resistance like SiC, Al_2O_3, and graphene. As a result of these stud-

*Corresponding author: e-mail address: ahmetoktay@gmail.com

Table 1. Components of samples produced by mechanical alloying (wt.%)

Sample ID	SiC	h-BN	Zn	Sn	Cu
A	0	0.25	10	10	Balance
B	0.25	0.25	10	10	Balance
C	0.50	0.25	10	10	Balance
D	1	0.25	10	10	Balance
E	2	0.25	10	10	Balance
F	4	0.25	10	10	Balance

ies, it has been observed that, depending on the ratios of these additives, there is a reduction in COF alongside an increase in wear resistance.

To our knowledge, no prior literature has been identified that addresses incorporating both Zn and Sn alloying elements, SiC, and solid lubricant h-BN into copper matrix metallic materials commonly used for sliding bearings.

Hence, in this study, ceramic particle-reinforced metal matrix composite sliding bearing alloys were produced by adding SiC in different ratios and h-BN to Cu, Sn, and Zn metallic powders, followed by high-temperature sintering. Characterization processes were carried out after conducting wear and friction tests on these prepared samples.

2. Experimental

Cu (NK272), Sn (NK225), Zn (NK222), and SiC (F600) powders used in the study were obtained from the Nanokar company with the specified code information. The purity of the alloy powders is 99.97 %, and their average particle size is approximately ~ 45 μm. The purity of SiC powders is also 99.97 %, with an average particle size of ~ 15 μm. The h-BN reinforcement material used in the study was obtained from the Chempounds company with the code NG04EO072390 and has a purity of 99.7 % and an average particle size of ~ 45 μm. The metallic powders, h-BN, and SiC powders in the quantities shown in Table 1 were subjected to a mechanical alloying process for 3 h at 1000 rpm. A high-energy ball mill with water cooling (Retsch Emax) was employed for the mechanical alloying process. The mill is equipped with a container made of 50 cm^3 of tungsten carbide (WC) and 8 WC balls with a diameter of 10 mm. Following mechanical alloying, the powder mixtures were compressed into cylindrical molds with a diameter of 20 mm under a pressure of 400 N mm^{-2}. The resulting samples were sintered in an atmosphere-controlled furnace under argon gas at 820 ℃ for 2 h.

Following sintering, dimensional changes on the samples were measured with a micrometer with a precision of ± 1 μm. The hardness of the post-sintered samples was determined using the Brinell method. Measurements were performed with a 2.5 mm diameter WC indenter under a load of 62.5 kg. The density of the sintered samples was measured using a Radwag AS220.R2 precision balance according to the Archimedes principle. During the measurements, the theoretical density of the final composition was calculated considering the theoretical densities of the components that make up the composition and compared with the measured density. Additionally, the porosity content within the sample was calculated using the theoretical density and the measured density.

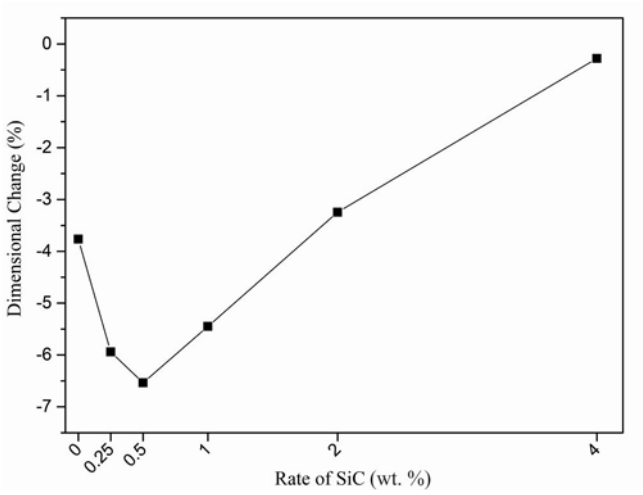

Fig. 1. Dimensional change in samples after sintering as a function of SiC ratio.

For microstructure analysis, a Philips XL30/SFEG Scanning Electron Microscope (SEM) was used, and chemical analyses in the map and spot modes were performed using the integrated Energy Dispersive Spectroscopy (EDS) unit. XRD analyses were conducted on a Bruker D8 Advance XRD device, using Cu Kα (graphite monochromator) radiation, with 40 kV and 40 mA, at a speed of 10° min^{-1} and intervals of 0.02° $step^{-1}$ in the range of 20°–100°.

Wear and friction tests were carried out on a Bruker UMT2 wear tester under loads of 1 and 3 N at a speed of 5 mm s^{-1} for a distance of 10 m. A 5 mm diameter WC ball was used during the tests. After the wear test, wear amounts and the topographic analysis of the worn surfaces were examined using a Zeiss Smartproof 5 optical profilometer.

3. Results and discussion

3.1. Dimensional changes

The dimensional change graph of the samples containing different amounts of SiC after sintering is shown in Fig. 1. After sintering, the sample without

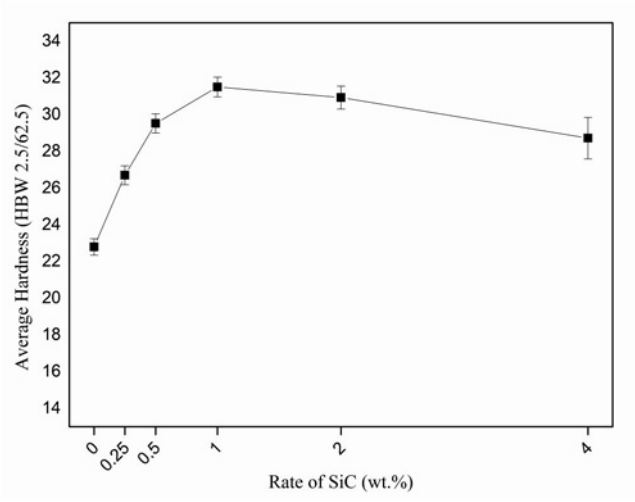

Fig. 2. Average hardness variation in the samples as a function of SiC ratio.

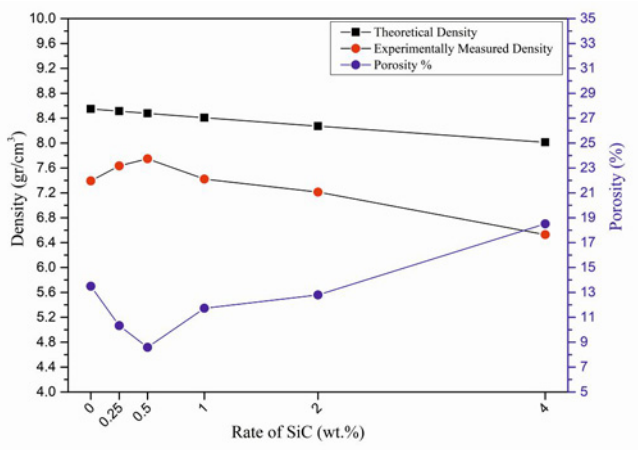

Fig. 3. Density change measured experimentally after sintering and calculated theoretically as a function of SiC content in the samples.

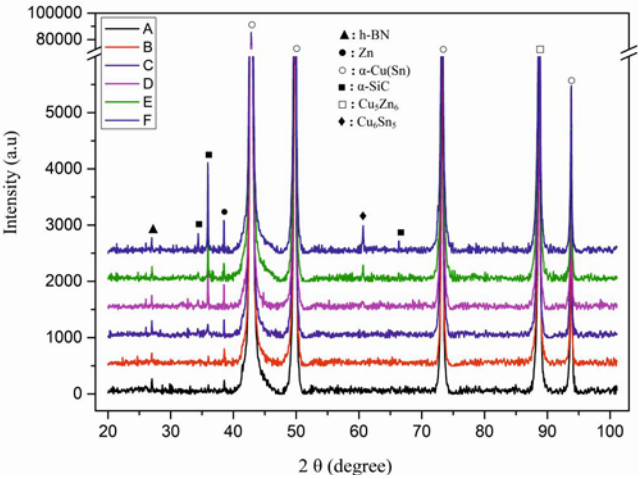

Fig. 4. XRD patterns obtained after sintering from samples containing varying amounts of SiC.

SiC exhibited approximately a 4 % shrinkage, adding 0.25 wt.% SiC, the shrinkage increased to approximately 6 %, and in the sample containing 0.5 wt.% SiC, it reached approximately 6.5 %. In samples with higher SiC content, it is observed that the shrinkage decreases linearly with an increase in SiC content, and in the sample with 4 % SiC, there is almost no significant dimensional change. One of the reasons for this phenomenon is that SiC particles, which have a high melting point, partially hinder diffusion by forming a barrier between the metal powder particles during sintering. The presence of SiC-rich structures with a network-like appearance among the metal powder particles after sintering in samples containing 2 and 4 % SiC generally supports these findings.

3.2. Hardness analysis

The change in average hardness after sintering as a function of SiC content is shown in Fig. 2. According to this figure, it can be observed that the hardness of the samples increased with the addition of 0.25, 0.5, and 1 wt.% SiC, while in samples with higher SiC content, hardness decreased with an increase in SiC content. This trend in hardness change with SiC content is consistent with similar studies reported in the literature [25]. The lowest hardness value, 23 HB, was observed in the sample without SiC, while the highest hardness value, 31 HB, was found in the sample containing 1 wt.% SiC. In samples with higher SiC content, a slight decrease in hardness was detected, with an average of 30 HB measured in the sample with the highest SiC content. Additionally, it is evident that there is increased scatter in hardness values for the sample containing 4 wt.% SiC. One of the reasons for the decrease in hardness in this sample and the increased scatter in hardness values is attributed to the partial disintegration of SiC-rich regions, leading to an increase in porosity content. This assessment is supported by microstructure analysis and density measurement results (Figs. 3 and 5).

3.3. Density change analysis

The density change measured experimentally and calculated theoretically according to the linear mixing rule, as a function of the SiC content, is shown in Fig. 3. The change in total porosity amount obtained by calculating the difference between the two densities is also depicted on the same graph (Fig. 3).

It is observed that the theoretically calculated density of the samples decreases with the SiC content in the samples. In addition, experimentally measured

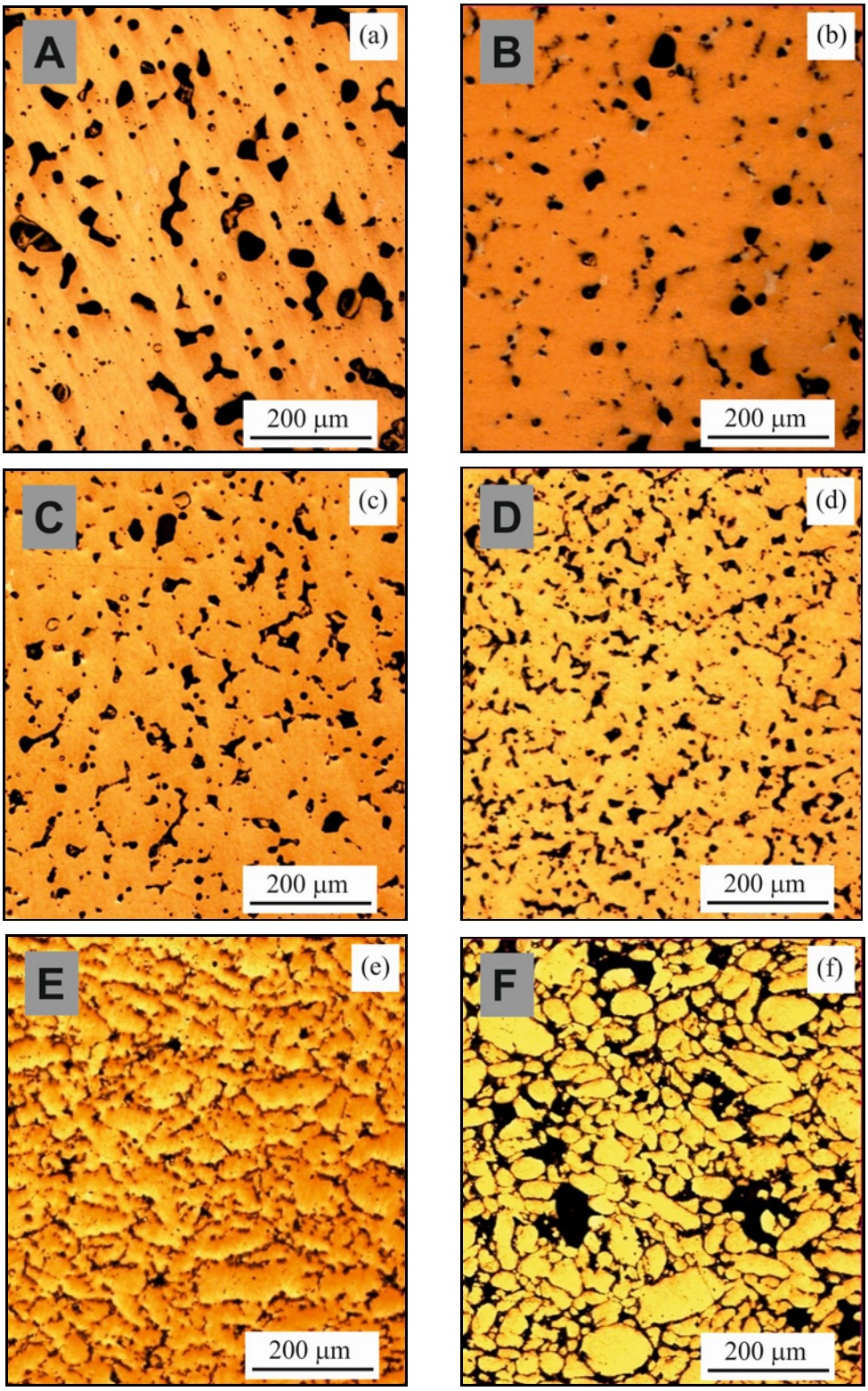

Fig. 5. OM images of the samples (A, B, C, D, E, and F) containing increasing ratios of SiC (Table 1) after sintering.

density values initially increased with the addition of SiC, but for samples containing more than 0.5 wt.%, the increase in SiC content led to a greater decrease in their theoretical densities. This phenomenon is attributed to the partial disintegration of SiC-rich regions identified in the microstructure, forming porous structures. The difference between the theoretically calculated density values and the experimentally mea-

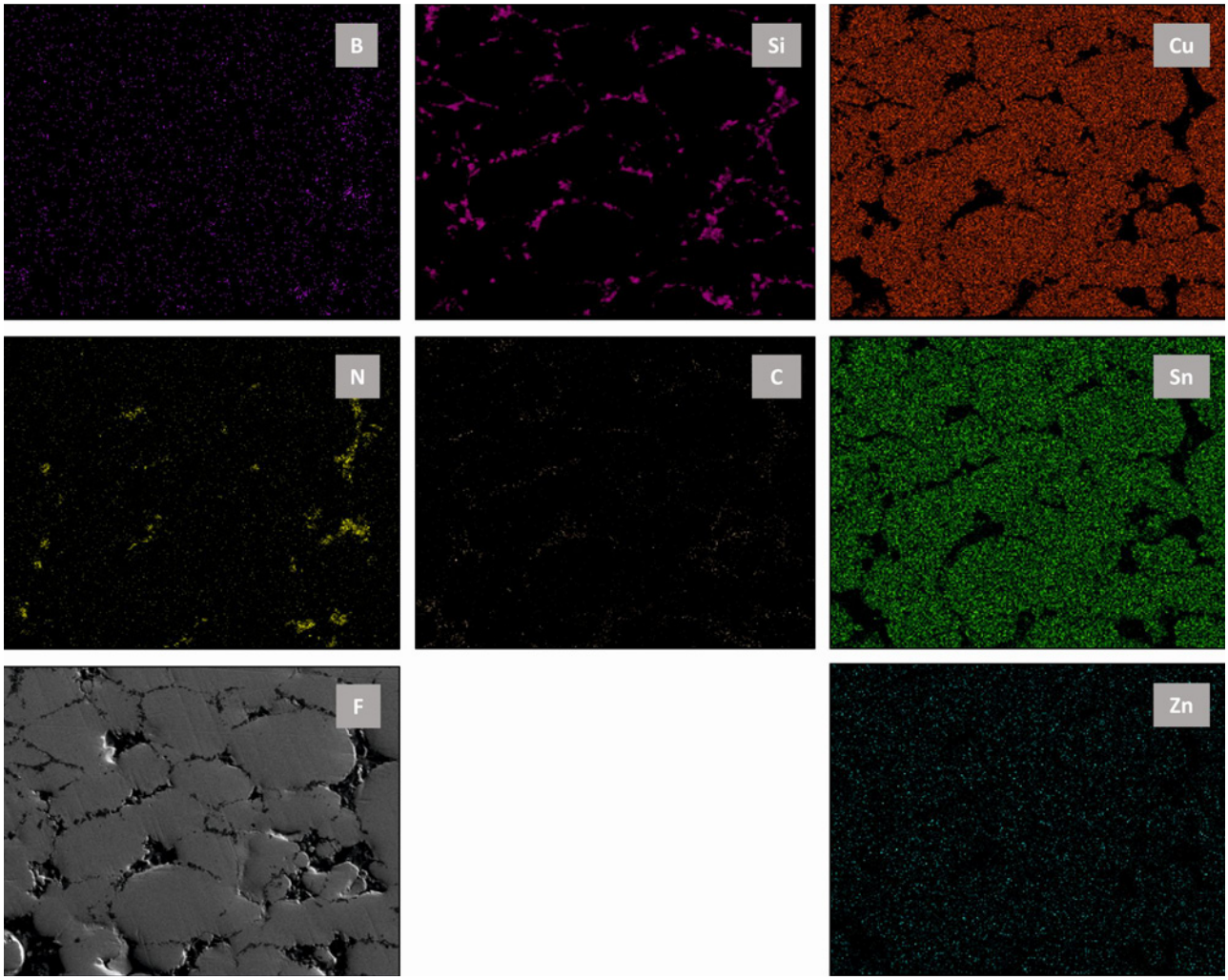

Fig. 6. The SEM image of the sample (F) containing 4 wt.% SiC and the SEM-EDS analysis result obtained in mapping mode.

sured density values is proportional to the sintering behavior in the samples and, consequently, the amount of porosity formed. Depending on the SiC content in the samples, the change in density and porosity after sintering parallels the hardness change in the samples (Fig. 2). A similar trend in density has been reported in other studies [25].

3.4. XRD analysis

The phases identified as a result of matching the peaks obtained from X-ray diffraction (XRD) analysis after sintering samples with different SiC content with the relevant database are depicted in Fig. 4. It has been determined that the characteristic peak at approximately 26° belongs to h-BN, and similar studies have reported the same result [26, 27]. Furthermore, the peaks at approximately 34° and 36° have been identified as belonging to SiC. It is observed that the intensities of these characteristic peaks increase with the increase in SiC content. It has been determined that the peak at approximately 39° in the XRD patterns of all samples belongs to Zn metal. Additionally, the characteristic peaks at approximately 43°, 50°, 74°, and 94° in the XRD patterns have been identified as belonging to Cu, which is the main component of the samples. Furthermore, the characteristic peaks at approximately 60° and 89° have been identified as corresponding to the Cu_6Sn_5 and Cu_5Zn_6 phases, respectively. These intermetallic phases are formed by solid-solid reactions during sintering.

3.5. Microstructure and SEM-EDS analysis

The optical microscope (OM) images of samples containing different amounts of SiC after sintering are provided in Fig. 5. It is observed that the SiC-free sample (A) was successfully sintered, but its microstructure contains independent pores. The amount of porosity in the microstructure appears to decrease with the addition and increase of SiC and increases with higher SiC content (Fig. 5f, sample F). The trend

in the change of pore quantities in the OM images appears to be like the change in pore quantities obtained from calculations (Fig. 3). It can be said that the addition of SiC prevents excessive pore growth up to a certain ratio. However, with further SiC addition, it is observed that SiC is distributed in a network-like structure among metallic matrix particles, hindering the sintering of metallic powders. Additionally, with the highest amount of SiC added, the largest pores are observed to form. It is believed that these pores are partially due to the disintegration of SiC. This observation is visible in the OM micrograph for the sample containing 4 wt.% SiC and is consistent with the findings of density change analysis and hardness values for that sample.

The SEM image taken from the sample containing 4 wt.% SiC (F) and the SEM-EDS analysis performed in mapping mode in the region where this image was obtained are presented in Fig. 6. In this sample, it is observed that Si and C, which constitute SiC, are distributed in a network-like structure, along with some partial agglomerations. Boron and nitrogen elements are present in agglomeration areas, indicating the presence of h-BN-rich structures and pores alongside these enriched structures. The SEM micrograph of the sample containing the highest amount of SiC, taken at different magnifications, is shown in Fig. 7. In Fig. 7, regions containing h-BN and SiC have been partially marked, considering the SEM-EDS results provided in Fig. 6. It can be inferred that the h-BN phase is located only within pores or among the grains and does not dissolve within the metallic matrix (Fig. 7). Additionally, it is hypothesized that in some regions entirely designated as pores, due to their soft structure, h-BN and SiC particles, come together due to the high sintering temperature, are not chemically bound to the sample during specimen preparation and are therefore dispersed/removed. However, it is understood from the microstructure that SiC particles are partially dispersed in the matrix and reduced to submicron sizes due to the mechanical alloying process.

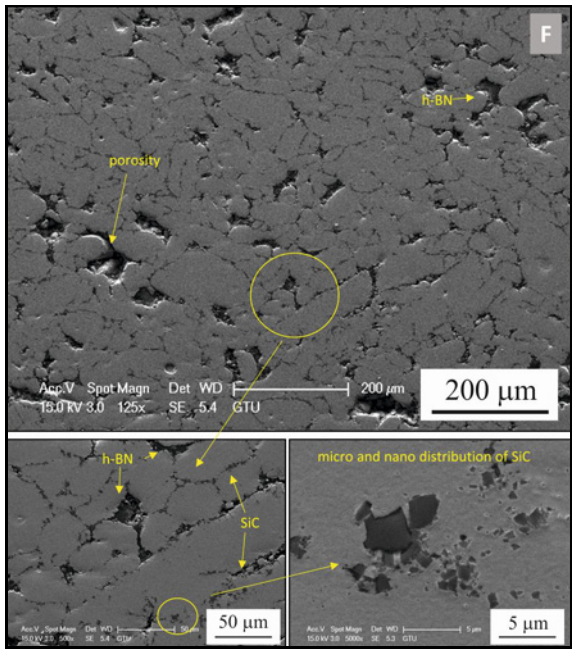

Fig. 7. SEM micrographs of the sample (F) containing 4 wt.% SiC showing detailed views and features of the microstructure at different magnifications.

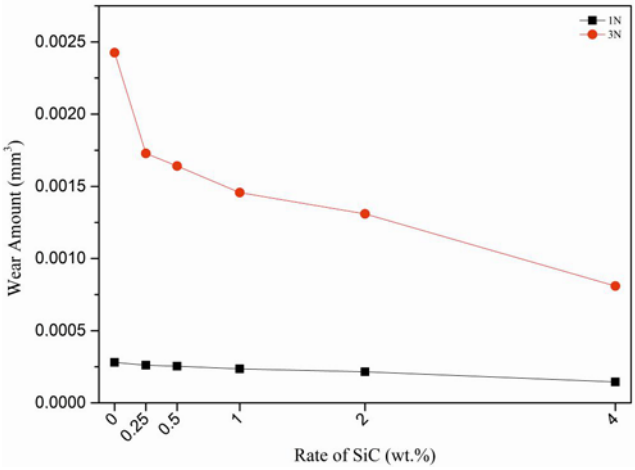

Fig. 8. Change in wear amount of the samples containing varying ratios of SiC under 1 and 3 N loads.

3.6. Wear tests

The change in wear amounts after the wear test at a speed of 5 m s^{-1} for 10 m under loads of 1 and 3 N, for samples containing varying ratios of SiC, is presented in Fig. 8. In general, it is observed that the wear amounts are higher in tests conducted under a 3 N load. However, increased SiC content reduces wear amounts for tests conducted with a 3 N load. Additionally, it is understood that an increase in SiC content during wear tests under a 1 N load does not lead to a significant change in wear amounts.

The OM images of wear tracks obtained after the wear tests are presented in Fig. 9. In tests conducted under a 3 N load, the width of the wear track is approximately ∼ 460 µm in the sample (A) without SiC, while it was determined that the width of the wear track partially decreases as the SiC content increases, with the sample (F) containing the highest SiC content having the smallest wear track width, which is approximately ∼ 250 µm. When evaluating the result of the wear track in sample A in conjunction with the change in density and porosity after sintering (Fig. 3), the higher wear amount in samples B and C is attributed to the abrasive ball contact surface. This is because sample A lacks SiC and has a coarse pore

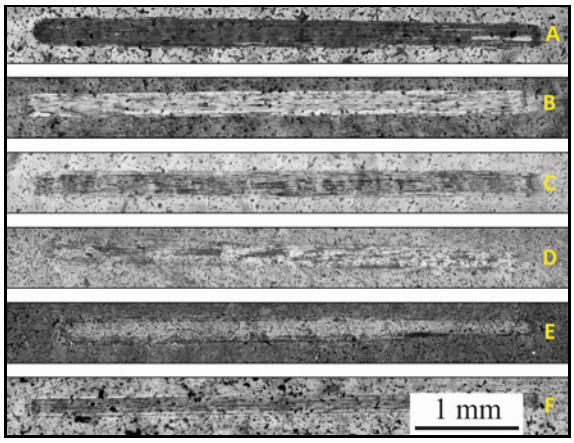

Fig. 9. OM images of the surfaces subjected to wear tests at a load of 3 N, a speed of 5 m s^{-1}, and a distance of 10 m for samples containing increasing rates of SiC.

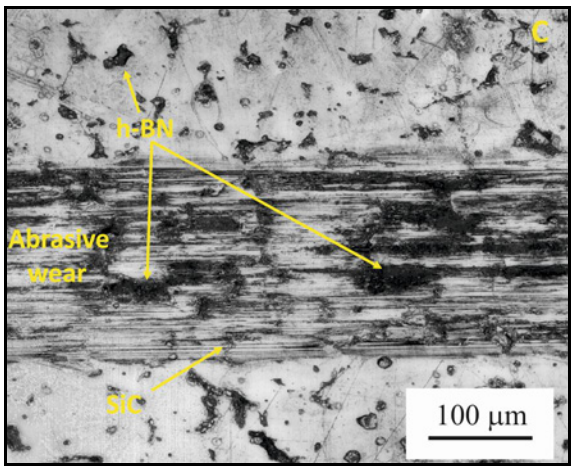

Fig. 10. OM images of the surfaces subjected to wear tests at a load of 3 N, a speed of 5 m s^{-1}, and a distance of 10 m for sample (C) containing 0.5 wt.% SiC.

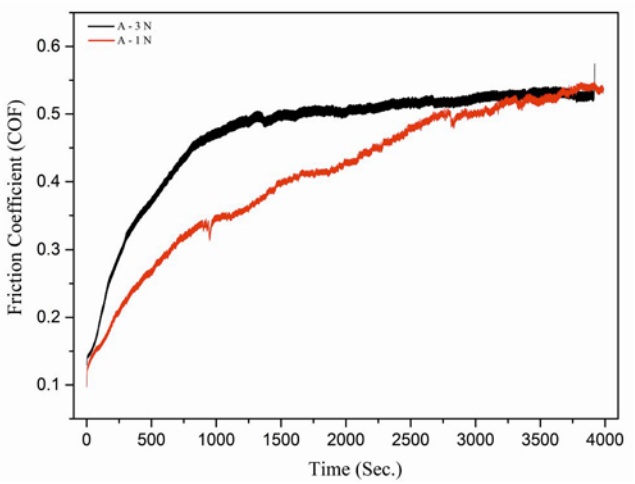

Fig. 11. Time-dependent changes in the COF for the SiC-free sample (A) under 1 and 3 N loads after wear tests.

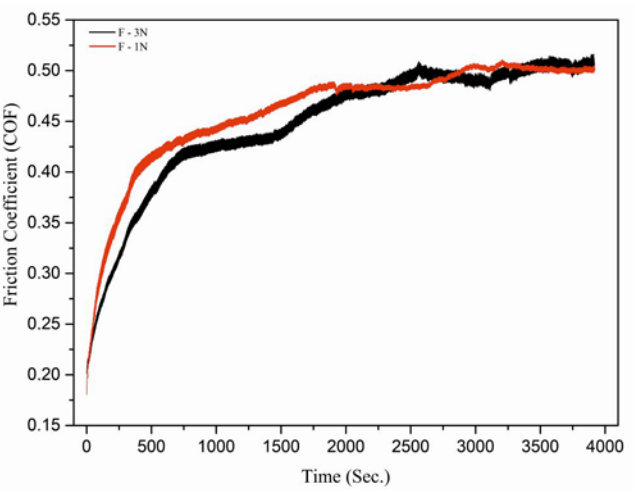

Fig. 12. Time-dependent changes in the COF for the sample (F) containing 4 wt.% SiC under 1 and 3 N loads after wear tests.

size, leading to non-uniform contact and increasing the contact surface. Furthermore, in samples E and F, characterized by a high SiC content, a noticeable reduction in both the width and continuity of the wear tracks is observed as SiC content increases during the wear test. This phenomenon can be attributed to the pronounced presence of SiC in certain areas and the dispersion of micro and nano-sized SiC particles within the metallic matrix, which imparts resistance to wear during testing. Moreover, the robust nature of SiC particles distributed within the matrix contributes to their detachment from the matrix during the wear test. This detachment results in the scratching of the softer matrix material and the formation of microcapillary grooves oriented parallel to the direction of the abrasive ball's movement (Fig. 10). Additionally, it was observed that the regions where h-BN particles cluster within the structure tend to smear between the abrasive ball and the matrix during the wear test. In studies where h-BN is employed as a solid lubricant, even with a different metallic phase, literature reports the occurrence of layered-type wear after wear tests [28].

The changes in COF during the wear tests for SiC-free (A) and 4 wt.% SiC-containing samples (F) under 1 and 3 N loads over 4000 s are presented in Figs. 11 and 12, respectively. It was observed that the final COF values remained relatively constant at around ~0.50 in wear tests conducted under both 1 and 3 N loads, irrespective of SiC content. Furthermore, it is possible to divide the COF change graph during the wear test for sample F into two independent regions.

In the first region (3 N for 500 s), a linear increase in COF can be observed, indicating abrasive wear independent of the load. In contrast, for sample A, it was observed that the COF measured during the wear test conducted under a 1 N load exhibited a continuously increasing trend, almost stabilizing by the end of the test. The COF increased rapidly and then exhibited a more horizontal trend, nearly remaining unchanged in the wear test performed under a 3 N load on the same sample. This phenomenon is believed to be due to a change in the wear mode between the abrasive ball and the samples. Indeed, it is inferred that the change in SiC content leads to a change in the wear mode, particularly evident in SiC-free sample (A) under low load (1 N), where abrasive wear is seen (Fig. 11). This situation indicates that in the SiC-free sample, as the load increases, the matrix undergoes excessive deformation, resulting in an expansion of the interaction areas/depth with the abrasive ball and causing a rapid increase in the COF. Literature reports a similar trend in the COF in studies where h-BN is employed as a solid lubricant, even with a different metallic phase. Initially, adding h-BN leads to a decrease in COF, but with an increase in the amount added, COF tends to increase [30]. Similar findings have been observed in studies using Mo_2S as a solid lubricant, where the wear rates initially decrease with the addition of the lubricant but increase as the amount added is further increased [29].

4. Conclusions

The added SiC particles were observed to disperse uniformly within the metallic matrix. Furthermore, influenced by mechanical alloying, these particles underwent fragmentation, resulting in dimensions below the micrometer scale, showcasing sub-micron attributes.

During sintering, the formation of Cu_5Zn_6 and Cu_6Sn_5 phases was identified. However, it was evident from XRD results that no reaction occurred between the Cu-Sn-Zn metallic phase, constituting the matrix, and the SiC and h-BN phases.

Upon sintering, notably in specimens containing 2 and 4 wt.% SiC, partial agglomeration was detected, likely facilitated by diffusion effects. In the case of 4 wt.% SiC samples, during sample preparation, partial spilling occurred, resulting in porosity formation.

The incorporated h-BN (0.25 wt.% constant for all samples) primarily exhibited clustered distribution within the matrix, with limited mechanical or chemical bonding to the matrix material.

Increased SiC content in sintered Cu-Sn-Zn sliding bearing alloys reduced dimensional change. In samples containing 4 wt.% SiC, there is virtually no change in sample dimensions.

The densities of sintered samples increased up to 0.5 wt.% SiC and then decreased with higher SiC ratios.

The average hardness in the sintered samples initially increased with higher SiC content. However, as SiC content increased, especially in the 4 wt.% SiC sample, hardness dropped to approximately 29 HB, and hardness-related standard deviation increased.

Following wear tests conducted under a 3 N load, it was ascertained that incorporating SiC reduced wear volume. Conversely, wear tests conducted under a 1 N load exhibited negligible discernible distinctions.

The wear tests revealed that the COF stabilized around 0.5 in the later stages, regardless of SiC inclusion. However, during the initial stages, samples without SiC and under a 1 N load exhibited a slower COF increase, eventually matching samples tested under a 3 N load. This suggests that SiC addition improved the matrix's mechanical properties, enhancing stability during testing.

Acknowledgements

This study is based on the doctoral research "Production and Characterization of SiC and h-BN Particle-Reinforced Cu-Sn-Zn Alloy Sliding Bearings by Powder Metallurgy" conducted at Yildiz Technical University (Istanbul).

References

[1] Magagnin Luca, Engineered Metal Matrix Composites: Forming Methods, Material Properties, and Industrial Applications, New York, 2012.

[2] S. Ilangovan, S Arul, Effect of Zn and Cu content on microstructure, hardness and tribological properties of cast Al-Zn-Cu alloys, International Journal of Engineering Research in Africa 27 (2016) 1–10. https://doi.org/10.4028/www.scientific.net/JERA.27.1

[3] B. Unlu, E. Atik, Evaluation of effect of alloy elements in copper based CuSn10 and CuZn30 bearings on tribological and mechanical properties, Journal of Alloys and Compounds 489 (2010) 262–268. https://doi.org/10.1016/j.jallcom.2009.09.068

[4] A. Zeren, E. Feyzullahoglu, M. Zeren, A study on tribological behaviour of tin-based bearing material in dry sliding, Mater. Design 28 (2007) 318–323. https://doi.org/10.1016/j.matdes.2005.05.016

[5] P. Jha, R. K. Gautam, R. Tyagi, Friction and wear behavior of Cu-4 wt.% Ni-TiC composites under dry sliding conditions, Friction 5 (2017) 437–446. https://doi.org/10.1007/s40544-017-0157-7

[6] E. Hong, K. Bradley, T. You, M.-S. Sun, Y.-S. Kim, H. Choe, Tribological properties of copper alloy based composites reinforced with tungsten carbide particles, Wear (2011) 591–592. https://doi.org/10.1016/j.wear.2011.01.015

[7] S. G. Sapate, A. Uttarwar, R. C. Rathod, Analyzing dry sliding wear behaviour of copper matrix composites reinforced with pre-coated SiC_p particles, Mater.

and Design (2009) 376–386.
https://doi.org/10.1016/j.matdes.2008.04.055
[8] T. E. Abioye, H. Zuhailawati, M. A. I. Azlan, A. S. Anasyiada, Effects of SiC additions on the microstructure, compressive strength and wear resistance of Sn-Sb-Cu bearing alloy formed via powder metallurgy, Mater. Res. Technol. 9 (2020) 13196–13205. https://doi.org/10.1016/j.jmrt.2020.08.102
[9] K. M Shoroworthi, T. Laoui, A. Haseeb, J. P. Celis, L. Froyen, Microstructure and interface characteristics of B_4C, SiC and Al_2O_3 reinforced Al matrix composites: a comparative study, J. Mater. Process Technol. 142 (2003) 738–43.
https://doi.org/10.1016/S0924-0136(03)00815-X
[10] A. Erdemir, Solid Lubricants and Self-Lubricating Films, B. Bhushan (Ed.), Modern Tribology Handbook, Materials Coating and Industrial Applications, CRD press, Florida, 2001, pp. 787–826.
[11] M. R. Akbarpoura, M. Najafia, S. Alipour, H. S. Kim, Hardness wear and friction characteristics of nanostructured Cu-SiC nanocomposites fabricated by powder metallurgy route, Materials Today Communications 18 (2019) 25–31.
https://doi.org/10.1016/j.mtcomm.2018.11.001
[12] K. Miyoshi, Solid lubrication fundamentals and applications, UK, Taylor & Francis, 2001.
[13] C. Busch, Solid lubrication, T. Mang, W. Dresel (Ed.), Lubricants and Lubrication, second ed., Weinheim, Wiley, 2007, pp. 694–714.
[14] A. R. Lansdown, Molybdenum Disulphide Lubrication, UK, Elsevier, 1999.
[15] B. Lin, D. Yi, H. Liu, J. Xu, B. Wang, High-temperature pre-sintering: A new strategy to improve the properties of h-BN/CuSn10 matrix composites, Journal of Alloys and Compounds 814 (2020) 152325. https://doi.org/10.1016/j.jallcom.2019.152325
[16] W. Hua, D. Yi, W. Wang, B. Lin, B. Wang, Experimental investigation of hardness and impact toughness of in suit Ag-rich binder phase formation with h-BN/CuSn10 metal matrix composite, Journal of Alloys and Compounds 859 (2021) 157859.
https://doi.org/10.1016/j.jallcom.2020.157859
[17] T. Li, D. Yi, J. Hu, J. Xu, J. Liu, B. Wang, Surface modification of h-BN and its influence on the mechanical properties of $CuSn_{10}$/h-BN composites, Journal of Alloys and Compounds 723 (2017) 345–353. https://doi.org/10.1016/j.jallcom.2017.06.264
[18] S. Zhu, J. Cheng, Z. Qiao, J. Yang, High temperature solid-lubricating materials: A review, Tribology International 133 (2019) 206–223.
https://doi.org/10.1016/j.triboint.2018.12.037
[19] A. T. Volochko, I. N. Rumyantseva, Thermal stability of aluminum composite materials containing sulfides of copper, molybdenum and zinc, Powder Metallurgy and Metal Ceramics 31 (1992) 446–448. https://doi.org/10.1007/BF00796258
[20] G. Stachowiak, A. Batchelor, Engineering Tribology, Elsevier, US, 2001.
[21] P. Ravindran, K. Manisekar, R. Narayanasamy, P. Narayanasamy, Tribological behaviour of powder metallurgy processed aluminium hybrid composites with the addition of graphite solid lubricant, Ceramics International 39 (2013) 1169–1182.
https://doi.org/10.1016/j.ceramint.2012.07.041
[22] H. Nautiyal, S. Kumari, O. P. Khatri, R. Tyagi, Copper matrix composites reinforced by rGO-MoS_2 hybrid: Strengthening effect to enhancement of tribological properties, Composites Part B 173 (2019) 106931. https://doi.org/10.1016/j.compositesb.2019.106931
[23] M. Rouhi, M. Moazami-Goudarzi, M. Ardestani, Comparison of effect of SiC and MoS_2 on wear behavior of Al matrix composites, Trans. Nonferrous Met. Soc. China 29 (2019) 1169−1183.
https://doi.org/10.1016/S1003-6326(19)65025-9
[24] J. Wu, Z. Li, G. Wen, Z. Gao, Y. Li, Y. Zhao, Friction mechanism analysis of copper-based composites reinforced with ball-milled and modified composite ceramic powders, Wear 528–529 (2023) 204959. https://doi.org/10.1016/j.wear.2023.204959
[25] H. Kato, M. Takama, Y. Iwai, K. Washida, Y. Sasaki, Wear and mechanical properties of sintered copper-tin composites containing graphite or molybdenum disulfide, Wear 255 (2003) 573–578.
https://doi.org/10.1016/S0043-1648(03)00072-3
[26] J. Duan, L. Li, Y. Tong, Z. Chen, D. Deng, J. Liu, Z. Cai, H. Wang, Core-shell structured h-BN@Ni reinforced CoCrNi-based self-lubricating composites, Surface and Coatings Technology 448 (2022) 128939 https://doi.org/10.1016/j.surfcoat.2022.128939
[27] C. Wu, C. Xu, C. Xiao, M. Yi, Z. Chen, H. Chen, An advanced self-lubricating ceramic composite with the addition of core-shell structured h-BN@Ni powders, International Journal of Refractory Metals and Hard Materials 72 (2018) 276–285. https://doi.org/10.1016/j.surfcoat.2022.128939
[28] J. Duan, L. Li, Y. Tong, Z. Chen, D. Deng, Z. Cai, H. Wang, J. Liu, Core-shell structured h-BN-Ni reinforced CoCrNi-based self-lubricating composites, Surface and Coatings Technology 448 (2022) 128939. https://doi.org/10.1016/j.surfcoat.2022.128939
[29] S. Lifan, G. Yuan, K. Dejun, Effect of MoS_2 mass fraction on microstructure and tribological characteristics of laser cladded Cu-10Al coating, Surfaces and Interfaces 28 (2022) 101599.
https://doi.org/10.1016/j.surfin.2021.101599
[30] H. Chen, G. Xiao, Z. Chen, M. Yi, J. Zhang, Z. Li, C. Hu, Hexagonal boron nitride nanosheets as lubricant additive to 5CB liquid crystal for friction and wear reduction, Materials Letters 307 (2022) 131007. https://doi.org/10.1016/j.matlet.2021.131007